

PAPER • OPEN ACCESS

## A splitting turbulence algorithm for mixing parameterization in the ocean circulation model

To cite this article: S N Moshonkin *et al* 2019 *IOP Conf. Ser.: Earth Environ. Sci.* **231** 012038

View the [article online](#) for updates and enhancements.

# A splitting turbulence algorithm for mixing parameterization in the ocean circulation model

S N Moshonkin<sup>1,2</sup>, V B Zalesny<sup>1,2</sup> and A V Gusev<sup>1,2,3</sup>

<sup>1</sup> Marchuk Institute of Numerical Mathematics of the Russian Academy of Sciences, Gubkina st. 8, 119333, Moscow, Russia

<sup>2</sup> Marine Hydrophysical Institute of the Russian Academy of Sciences, Kapitanskaya st. 2, 299011, Sevastopol, Russia

<sup>3</sup> P.P.Shirshov Institute of Oceanology of the Russian Academy of Sciences, Nakhimovsky av. 36, 117997, Moscow, Russia

E-mail: [anatoly.v.gusev@gmail.com](mailto:anatoly.v.gusev@gmail.com)

**Abstract.** A new algorithm is proposed for solving the  $k$ - $\omega$  turbulence equations embedded in the Ocean general circulation model (OGCM). Both the circulation and turbulence models are solved using the splitting method with respect to physical processes. We split the turbulence equations into the two stages describing transport–diffusion and generation–dissipation processes. At the generation–dissipation stage, the equation for  $\omega$  does not depend on turbulent kinetic energy (TKE)  $k$ . It allows us to solve both turbulence equations analytically. The technique allows us to use the same time step as in the OGCM that ensures high computational efficiency. The OGCM has a horizontal resolution of 0.25 degree and 40 sigma-levels along the vertical. The coupled model is used to simulate the hydrophysical fields of the North Atlantic and Arctic Ocean. Using the analytical solution for the  $k$ - $\omega$  turbulence model increases adequacy in reproducing oceanic characteristics by varying coefficients of this solution in numerical simulations. We present the assessments of sensitivity to variations in TKE inflow at the ocean surface. A high sensitivity of the ocean vertical structure to variations in the analytical solution coefficients is revealed at the generation–dissipation stage. In the analytical solution, we use the stability function obtained with solving the Reynolds equations. This improves reproduction of the Arctic upper desalination layer and North Atlantic and Nordic Seas upper quasi-homogeneous layer depth, comparing to using the simple form of the Prandtl number dependence on the Richardson number.

## 1. Introduction

At present, the two approaches are predominant in the primitive ocean general circulation models (OGCMs) to determining the vertical turbulent exchange coefficients for momentum  $K_U$ , heat  $K_T$ , and salt  $K_S$  in the problems of climate variability simulation. In the first one, the coefficients are defined as functions of stratification and velocity shear, or local Richardson number. This approach is used, e.g., in the Earth system model [1]. The second approach uses the so-called two-equation turbulence models [2]. The first equation here is the one for the turbulent kinetic energy (TKE)  $k$ . The second one closing the system is an equation for turbulence scale  $l$  ( $k - kl$  closure), or for the specific dissipation rate  $\epsilon$  of TKE ( $k - \epsilon$  closure), or for the frequency characteristic  $\omega$  of TKE dissipation ( $k - \omega$  closure). The characteristics  $l$ ,  $\epsilon$  and  $\omega$  are related algebraically. In the scope of the two-equations turbulence model approach, one can describe,



e.g., influence of Langmuir vortices and Stokes wave transport on mixing [3]. Along with the developed turbulence parameterization in the upper layer, it is possible to describe processes of underdeveloped turbulence in seasonal and basic pycnoclines, deep ocean mixing (double diffusion, tidal effects on the relief) [4].

We are developing the second approach and focus our attention on improving the numerical method for solving the turbulence equations. The OGCM and turbulence equations are solved using the unified method, which is the multicomponent splitting algorithm. The algorithm includes splitting by physical processes and spatial coordinates. The turbulence model is formulated in terms of the  $k - \omega$  parameterization, since using this approach, the algorithm for solving split turbulence equations is the most effective.

## 2. Turbulence model equations and a solution method

We use the isobatic sigma coordinate system:  $\sigma = (z - \zeta)/(H - \zeta)$ , where  $z$  is geopotential vertical coordinate,  $H$  is depth of the undisturbed ocean,  $\zeta$  is sea surface height (SSH). The turbulence equations in terms of  $k - \epsilon$  and  $k - \omega$  have the form [2]:

$$\begin{aligned} \frac{dk}{dt} - \frac{1}{Z_\sigma^2} \frac{\partial}{\partial \sigma} \left( \frac{K_U}{\sigma_k} \frac{\partial k}{\partial \sigma} \right) - \Lambda k &= K_U G^2 - K_T N^2 - \epsilon, \\ \frac{d\epsilon}{dt} - \frac{1}{Z_\sigma^2} \frac{\partial}{\partial \sigma} \left( \frac{K_U}{\sigma_\epsilon} \frac{\partial \epsilon}{\partial \sigma} \right) - \Lambda \epsilon &= \left[ c_1^\epsilon K_U G^2 - c_3^\epsilon K_T N^2 - c_2^\epsilon \epsilon \right] \frac{\epsilon}{k}, \\ \frac{dk}{dt} - \frac{1}{Z_\sigma^2} \frac{\partial}{\partial \sigma} \left( \frac{K_U}{\sigma_k} \frac{\partial k}{\partial \sigma} \right) - \Lambda k &= K_U G^2 - K_T N^2 - (c_S^0)^4 \omega k, \\ \frac{d\omega}{dt} - \frac{1}{Z_\sigma^2} \frac{\partial}{\partial \sigma} \left( \frac{K_U}{\sigma_\omega} \frac{\partial \omega}{\partial \sigma} \right) - \Lambda \omega &= \left[ c_1^\omega K_U G^2 - c_3^\omega K_T N^2 - c_2^\omega (c_S^0)^4 k \omega \right] \frac{\omega}{k}, \end{aligned} \quad (1)$$

here  $Z_\sigma = H - \zeta$ ,  $G$  and  $N$  are frequencies of the velocity shear and buoyancy,  $\Lambda$  is horizontal diffusion operator. Values of the parameters  $c_1^\epsilon$ ,  $c_2^\epsilon$ ,  $c_3^\epsilon$ ,  $c_1^\omega$ ,  $c_2^\omega$ ,  $c_3^\omega$ ,  $c_S^0$  are given in [2].

To solve (1), we use the method of splitting by physical processes. The complete equation set is split into two stages: transport–diffusion and generation–dissipation. At the transport–diffusion stage, we have:

$$\frac{dk}{dt} = \frac{1}{Z_\sigma^2} \frac{\partial}{\partial \sigma} \left( \frac{K_U}{\sigma_k} \frac{\partial k}{\partial \sigma} \right) + \Lambda k, \quad \frac{d\epsilon}{dt} = \frac{1}{Z_\sigma^2} \frac{\partial}{\partial \sigma} \left( \frac{K_U}{\sigma_\epsilon} \frac{\partial \epsilon}{\partial \sigma} \right) + \Lambda \epsilon, \quad \frac{d\omega}{dt} = \frac{1}{Z_\sigma^2} \frac{\partial}{\partial \sigma} \left( \frac{K_U}{\sigma_\omega} \frac{\partial \omega}{\partial \sigma} \right) + \Lambda \omega.$$

As the main boundary condition on the upper ocean boundary, for TKE we use:

$$-\frac{K_U}{Z_\sigma \sigma_k} \frac{\partial k}{\partial \sigma} = C_g \left( u_*^S \right)^3,$$

where  $u_*^S$  is friction rate at the ocean surface,  $C_g$  is dimensionless parameter of wind generation. Note that most often its values are taken equal to 40 [3] or 10 [5]. Next, we study the solution sensitivity to this parameter.

At the generation–dissipation stage, we have the equations:

$$\begin{aligned} \frac{\partial k}{\partial t} &= \left[ (c_S^0)^4 \left( G^2 - \frac{N^2}{\text{Pr}} \right) \frac{k}{\epsilon} - \frac{\epsilon}{k} \right] k, \quad \frac{\partial \epsilon}{\partial t} = \left[ (c_S^0)^4 \left( c_1^\epsilon G^2 - c_3^\epsilon \frac{N^2}{\text{Pr}} \right) \frac{k}{\epsilon} - c_2^\epsilon \frac{\epsilon}{k} \right] \epsilon, \\ \frac{\partial k}{\partial t} &= \left[ (c_S^0)^4 \left( G^2 - \frac{N^2}{\text{Pr}} \right) \frac{1}{\tilde{\omega}} - \tilde{\omega} \right] k, \quad \frac{\partial \tilde{\omega}}{\partial t} = \left[ (c_S^0)^4 \left( c_1^\omega G^2 - c_3^\omega \frac{N^2}{\text{Pr}} \right) \frac{1}{\tilde{\omega}} - c_2^\omega \tilde{\omega} \right] \tilde{\omega}, \end{aligned} \quad (2)$$

where  $\tilde{\omega} = (c_S^0)^4 \omega$ . The following relations are also used:  $K_U = (c_S^0)^3 C_S^U \frac{k^2}{\epsilon}$ ,  $K_T = \frac{K_U}{\text{Pr}}$ , where  $\text{Pr}$  is the Prandtl number,  $C_S^U$  is dimensionless stability function for momentum.

It can be seen that at the generation–dissipation stage, TKE is posed in the right-hand side of the  $k - \epsilon$  model (as well as for the  $k - kl$  model). In the  $k - \omega$  model, the equation for  $\omega$  does not depend on TKE, and it can be solved both numerically and analytically! It is the second way that ensures the high efficiency of the algorithm. The analytical solution of (2) has the form:

$$\omega = -r_d(r_m + r_p a_r)/(r_m - r_p a_r), \quad k = k^0 \left( \frac{E_1}{E_2} \right)^{\frac{A}{2B}} \left( \frac{E_3}{E_4} \right)^{\frac{D}{2C}}, \quad (3)$$

where

$$r_d = \sqrt{B/C}, \quad r_m = \omega^0 - r_d, \quad r_p = \omega^0 + r_d, \quad a_r = \exp(2\sqrt{BC} \cdot t), \\ E_1 = (r_m + r_p a_r)^2, \quad E_2 = 4(\omega^0)^2 a_r, \quad E_3 = 4r_d^2 a_r, \quad E_4 = (r_m - r_p a_r)^2, \\ C = c_S^\omega (c_S^0)^4, \quad D = (c_S^0)^4,$$

$\omega_0$  and  $k_0$  are the values at the initial moment (at the generation–dissipation stage).

The coefficients  $A$  and  $B$  can be calculated using two options:

$$A = (C_S^U G^2 - C_S^\rho N^2)/c_S^0, \quad B = (c_1^\omega C_S^U G^2 - c_3^\omega C_S^\rho N^2)/c_S^0, \quad (4)$$

or

$$A = C_S^U (G^2 - N^2/\text{Pr})/c_S^0, \quad B = C_S^U (c_1^\omega G^2 - c_3^\omega N^2/\text{Pr})/c_S^0. \quad (5)$$

Here  $C_S^U$  is dimensionless stability function for the momentum transport,  $C_S^\rho = C_S^T$  is stability function for scalar ( $T$  and  $S$ ) transport, and  $c_S^0$  is value of these functions for neutral stratification. An algorithm using the analytic solution (3) for turbulence equations is referred to as "splitting turbulence algorithm" (STA). Note one more feature of the proposed approach: - one can "control" the solution through the coefficients  $A$  and  $B$ . This is important for oceanological aspects of the ocean climate simulation with the OGCM.

Now consider the sensitivity of the solution to the variations of the coefficients  $A$  and  $B$ , particularly, to the choice of the calculation options (4) or (5), as well as to the choice of the function  $C_S^\rho = C_S^T$  or Prandtl number  $\text{Pr}$ . Let us the following dimensionless functions:

$$\alpha_G = \frac{1}{(c_S^0)^2} \frac{G^2}{\omega^2}, \quad \alpha_N = \frac{1}{(c_S^0)^2} \frac{N^2}{\omega^2}.$$

The prognostic equations for Reynolds stresses and turbulent heat fluxes assuming local equilibrium of stresses and heat fluxes can be represented as equations for the stability functions  $C_S^U$  and  $C_S^T$  in the form [6, 7]:

$$\begin{aligned} a_{11} C_S^U + a_{12} C_S^T &= b_1, \\ a_{21} C_S^U + a_{22} C_S^T &= b_2, \end{aligned} \quad (6)$$

where the coefficients have the form:

$$\begin{aligned} a_{11} &= 2.0424\alpha_G, & a_{12} &= 1 + 15.2958\alpha_N, & b_1 &= 1.0465, \\ a_{21} &= 1 + 2.5392\alpha_G + 3.0636\alpha_N, & a_{22} &= 8.1142\alpha_N, & b_2 &= 0.9888. \end{aligned}$$

Restrictions on the both free convection development and turbulence degeneration impose limitations on the magnitude of the coefficients [7]:

$$\alpha_N \geq -0.64, \quad \alpha_G \leq 1.65 + 25\alpha_N.$$

The solution of (6) has the form:

$$\begin{aligned}
C_S^U &= (c_6 + c_7\alpha_N)/d, \quad C_S^T = (c_8 + c_9\alpha_G + c_{10}\alpha_N)/d, \\
c_1 &= 1.0, \quad c_2 = 18.3594, \quad c_3 = 46.8602, \quad c_4 = 2.5392, \quad c_5 = 38.8391, \\
c_6 &= 0.9888, \quad c_7 = 6.6330, \quad c_8 = 1.0465, \quad c_9 = 3.2061, \quad c_{10} = 0.6377, \\
d &= c_1 + (c_2 + c_3\alpha_N)\alpha_N + (c_4 + c_5\alpha_N)\alpha_G \neq 0.
\end{aligned} \tag{7}$$

In the simulations below, we use two versions of STA. In the first one, we use the formulae (4) and (7). In the second one, we use formula (5) and the two assumptions. The first one [7] implies that

$$C_S^U = c_S^0, \tag{8}$$

the second one implies that the Prandtl number is a function of the Richardson number  $Ri = N^2/G^2$  [8]:

$$Pr = \begin{cases} 1, & Ri \leq 0.2; \\ 5Ri, & 0.2 < Ri < 2; \\ 10, & Ri \geq 2 \end{cases} \tag{9}$$

The  $k$ - $\omega$  turbulence model (1) is embedded in the OGCM referred to as Institute of Numerical Mathematics Ocean Model (INMOM). The INMOM equations are written in a sphere-based bipolar orthogonal  $\sigma$ -coordinate system. The sphere poles are placed to the geographical equator at 120°W and 60°E. The prognostic variables of the model are velocity horizontal components, SSH, potential temperature and the salinity. Horizontal turbulent tracer mixing is described as diffusion along geopotential surfaces. The coefficients of large-scale lateral diffusivity are assumed the same for temperature and salinity and equal to 10<sup>2</sup> m<sup>2</sup>/s. The model takes into account river runoff, as well as sea ice dynamics and thermodynamics.

Vertical mixing is described by a second-order operator. The exchange coefficients in the case of developed turbulence have the form:

$$K_U = \frac{C_S^U}{c_S^0} k, \quad K_T = \frac{C_S^T}{c_S^0} k, \quad K_S = K_T, \tag{10}$$

where  $k$  and  $\omega$  in (10) are calculated with the turbulence model (1) using solution (3). By unstable stratification of the potential density, high values of vertical viscosity and diffusion coefficients are set equal to 0.5 m<sup>2</sup>/s. With intermittent turbulence  $k < k_{min}$  [7], low background values of viscosity and diffusivity are set.

A more detailed description of the model and numerical algorithms for its solution based on the multicomponent splitting method are given in [9].

### 3. Numerical simulations

The model domain includes the Atlantic Ocean to the north of 30°S, the Arctic Ocean and Bering Sea. Open boundaries pass through 30°S and passages of the Aleutian Islands. In addition, the area includes the Mediterranean, Black and Baltic Seas. The grid spacing in latitude and longitude is 0.25° (620×440 nodes). 40  $\sigma$ -levels are set along the vertical with refinement near the surface. Bottom topography [10] is smoothed according to the model horizontal resolution to reduce low-scale bottom details. The model depth is limited to a minimum value of 10 m. The boundary conditions at the ocean surface were calculated using the atmosphere characteristics from the CORE-II dataset [11] for the period 1948–2009. Fluxes of heat, fresh water and

**Table 1.** Experiments and variations of parameters.

Experiment	$A$ and $B$ in (3)	$C_g$	$\tau_T$
EC40	(4), (7)	40	5 min
EC10	(4), (7)	10	5 min
EP40	(5), (8), (9)	40	1 hour
EC1h	(4), (7)	40	1 hour

momentum are calculated with using the CORE-2 data on air temperature, humidity, wind speed components and sea level pressure with a discreteness of 6 hours, long- and shortwave radiation with discreteness of 1 day, precipitation and river runoff with a discreteness of 1 month. The model sea surface temperature (SST) is used to compute surface heat fluxes. For shortwave radiation, its deep penetration is taken into account.

The initial conditions are climatic January fields of ocean temperature and salinity, rest state and sea ice null.

In numerical experiments for INMOM (OGCM), the time step  $\tau_{ocm}$  was equal to 1 hour. At the stage of transport–diffusion splitting, the  $k - \omega$  turbulence equations were also solved with a time step equal to 1 hour. When solving them at the stage of generation–dissipation, the time step  $\tau_T$  varied from 5 minutes to  $\tau_T = \tau_{ocm} = 1$  hour (see below).

In order to demonstrate the sensitivity of the ocean vertical structure to variations in the parameters, the simulations were carried out with the boundary conditions fitting to the particular year, taking into account the entire spectrum of synoptic perturbations of the characteristics of the atmosphere at the ocean surface. The model profiles  $T(z)$  and  $S(z)$  were obtained for different values of the parameters and the corresponding profiles from the Atlas of the Oceans [12, 13] were taken for comparison with model ones. July is chosen, when at a relatively small value of a quasi-homogeneous layer, the vertical structure is the most sensitive to variations in the parameters. The Arctic basin is chosen as the area for analysis.

The table 1 shows the characteristics of experiments with the INMOM when using STA in the turbulence model. In the EC40, the coefficients  $A$  and  $B$  in STA were also taken in the form (4) with the stability functions in the form (7) with the wind generation parameter  $C_g = 40$ . The EC10 differs from the EC40 only in that  $C_g = 10$ . In the EP40,  $A$  and  $B$  are used in the form (5) taking into account the Prandtl number in the form (9) with the stability function for momentum in the form (8). At the same time,  $C_g = 40$  in EP40. The EC1h is similar to the EC40, but the stability functions in EC1h are equal to their values at the time moment  $t_j$  and do not change over a time interval  $(t_j, t_{j+1})$  equal to the step  $\tau_{ocm}$  of the OGCM. That is,  $A = A_j$  and  $B = B_j$  in the form (4) on the interval  $(t_j, t_{j+1})$  and they are time-independent.

Fig. 1 shows the vertical structure of the ocean upper layer in July at the North Geographic Pole in the Transpolar Drift zone. The high sensitivity of the model profiles  $T(z)$  and  $S(z)$  is revealed to the change of parametrization variants. The stability of the upper layer stratification here is mainly related to the salinity vertical distribution. TKE inflow into the ocean at the surface is four times smaller in the EC10 than in EC40 that leads to a weaker mixing. The waters desalinated by ice melting and river runoff penetrate to a smaller depth, and in the EC10 a layer 0–15 m is reproduced, where the salinity is 0.6–0.9 PSU lower than in the E40. Salinity in the EC10 is higher than in the EC40, below the 15 m level in the halocline due to a lack of TKE and mixing with the upper freshened layers (fig. 1a). This also causes the reproduction in the EC10 of a higher water temperature in June into the upper 25 m than in the EC40 (fig. 1b). In general,  $S(z)$  and  $T(z)$  in the EC40 are closer to climatic data than in EC10.

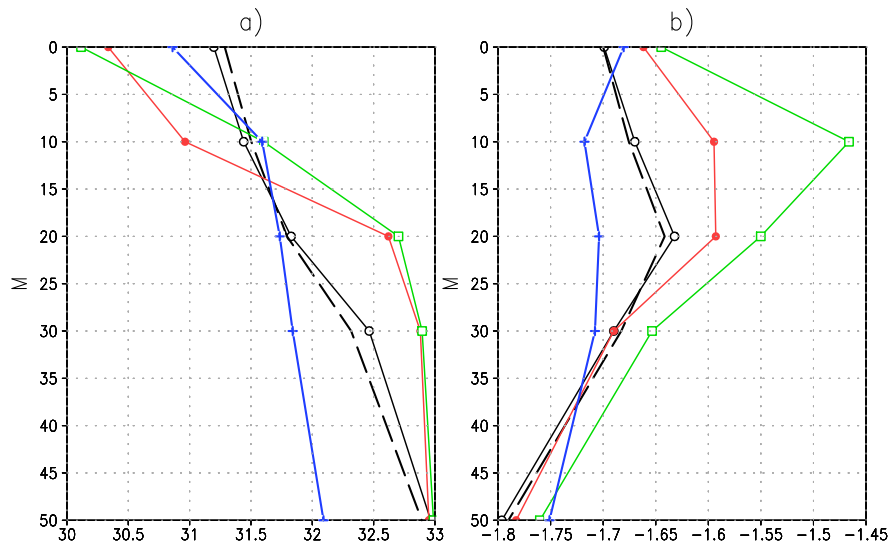


**Figure 1.** Salinity in PSU (a) and temperature in  $^{\circ}\text{C}$  (b) at the North Geographical Pole. July, layer 0–50 m. Blue solid is climate [12, 13]. Experiments: black solid is EC40, black dashed is EC1h, red is EC10, green is EP40.

When using the stability functions in the form (7), the model solution better corresponds to the observation data than when specifying the Prandtl number as a function of the Richardson number (9) in the EP40 (fig. 1). For EP40, desalination takes place in the near-surface layer, as in the EC10. At the same time, in the EP40 in the 0–20 m layer, both salinity gradient and water temperature are noticeably overestimated; there is an overestimated thermal inversion (fig. 1b). In general, it can be said that the variant EP40 corresponds to a reduced TKE inflow. An important element in the Arctic basin circulation is the Beaufort Gyre. It is well reproduced in the SSH field by the INMOM with the  $k - \omega$  turbulence model. The response of the vertical structure of the upper layer in the Beaufort Gyre to the change in the variants of parameters EC40, EC10, EP40 and EC1h is similar to the one shown in fig. 1. As well, there is an overestimated desalinated layer at the surface and overestimated salinity gradients in the upper 30 m for the EC10 and EP40 due to a lack of TKE.

In general, one can say that the EP40 corresponds to a reduced TKE. Indeed, an analysis of the TKE distribution in the 0–20 m layer showed that in the two marked regions of the Arctic, TKE in EC40 is about  $30 \text{ cm}^2/\text{s}^2$ , and for the EP40, it is  $5\text{--}15 \text{ cm}^2/\text{s}^2$ . Note, however, that in certain physical conditions and areas in the EP40, TKE was reproduced in the upper layer close to and even larger than in the EC40.

We especially note the low sensitivity of the ocean vertical structure by transition from the EC40 to the EC1h. The analytical solution (3) in the EC40 uses the time step 5 min, while in EC1h, it uses the time step of the OGCM equal to 1 hour. This indicates a high numerical efficiency of the proposed approach. For instance, the mean computational time at 8 processors for the EC40 of one physical day is 2.26 min, while this time is 1.57 min for the EC1h.

The upper quasi-homogeneous layer (UQL) thickness is an important characteristic of the mixing process in the ocean. To determine the UQL sensitivity to variation of parameters, the period of maximum free convection development was chosen. Fig. 2 shows the UQL thickness for December in the North Atlantic and Arctic Ocean in the EC40 and EP40. A high sensitivity of the UQL thickness to variations in the coefficients  $A$  and  $B$  in the analytical solution (3) is

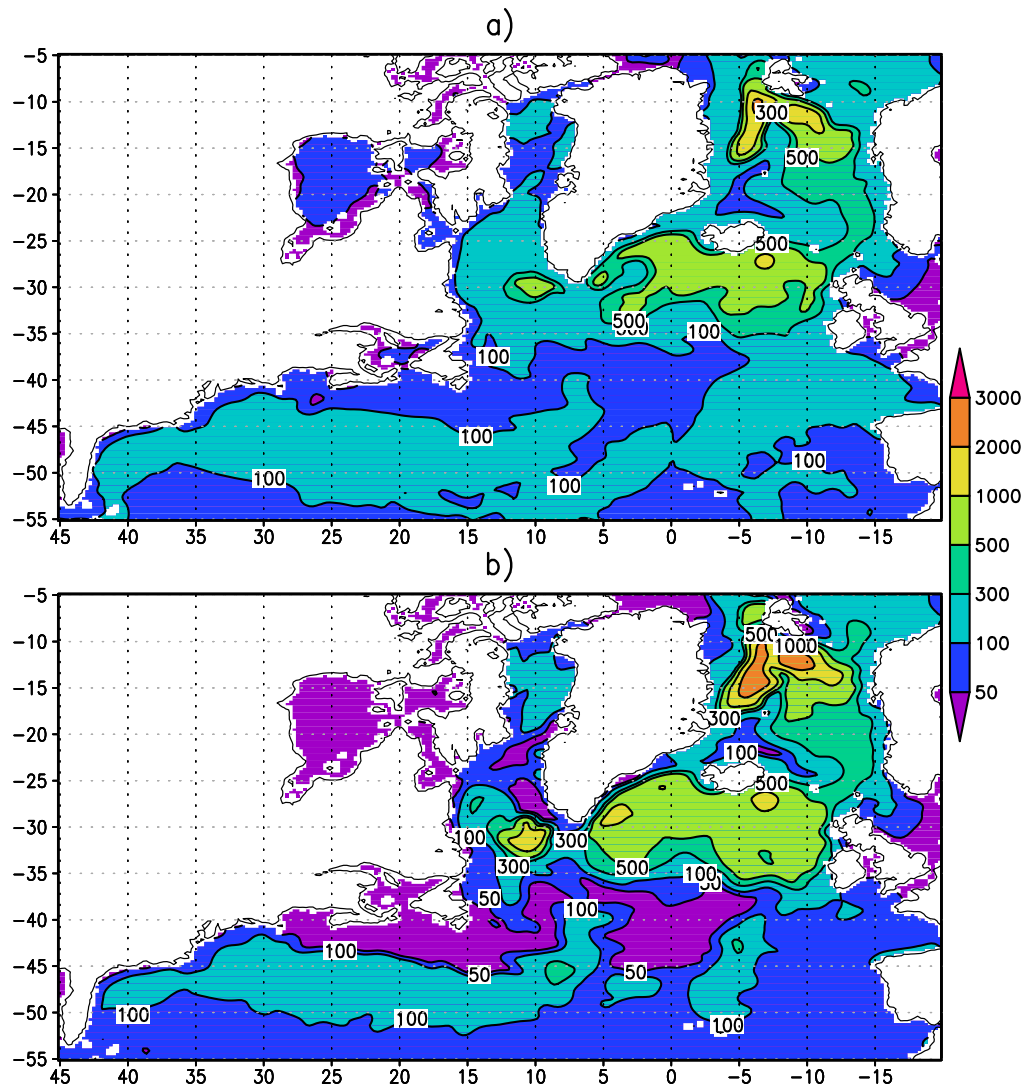


**Figure 2.** Upper quasi-homogeneous layer (UQL) thickness in meters, December. Experiments EC40 (a) and EP40 (b), model coordinates (see text). Within the UQL, water potential density differs from its surface value by less than  $0.15 \text{ kg/m}^3$ .

also seen. The difference in the UQL thickness between EC40 and EP40 is tens of meters in the mid-latitudes and hundreds of meters in the Nordic Seas. The variant with the coefficients of the analytical solution (3) in the form (4), (7) (experiment EC40) corresponds to the generalized observational data [14] better than the variant with the ones in the form (5), (8), (9) (experiment EP40). The use of a simple Prandtl number form as a function of the Richardson number underestimates the UQL thickness in the North Atlantic Current and overestimates it in the Nordic Seas (fig. 2).

Spatial distributions of the TKE in the upper layer is shown for the Nordic Seas (fig. 3). The characteristic of sensitivity to the time step for the solution of the turbulence equations with using the STA is appreciated here in terms of TKE. Transition from the step of 5 min in the EC40 (fig. 3a) to the step of 1 hour in the EC1h (fig. 3b) leads to the TKE change up to

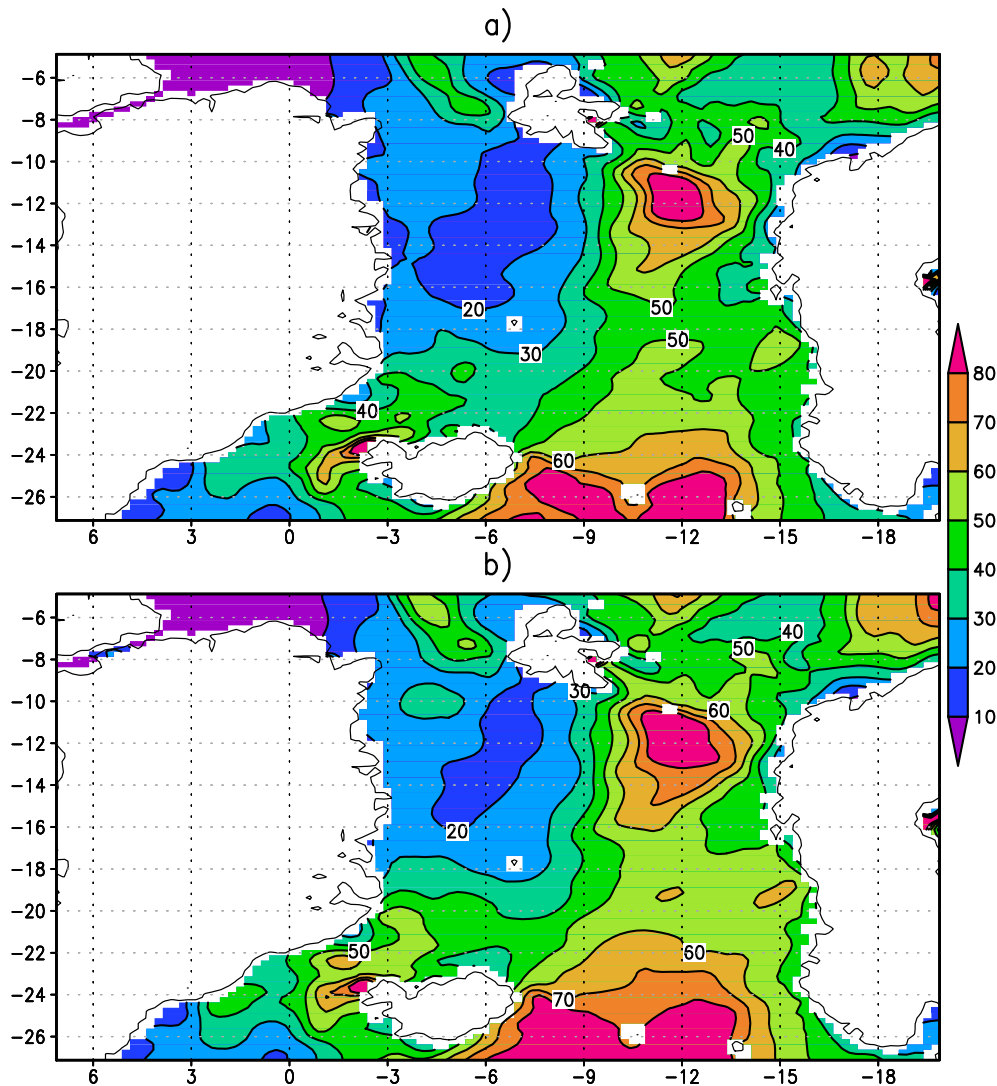


**Figure 3.** Turbulent kinetic energy in  $\text{cm}^2/\text{s}^2$  in the Nordic Seas, June. Layer 0–50 m. Experiments EC40 (a) and EC1h (b), model coordinates (see text).

$10 \text{ cm}^2/\text{s}^2$  in certain regions. However, a good agreement in TKE distribution is seen in the both experiments. One can state a relatively low TKE sensitivity to the change in time step when solving the turbulence equations. That confirms a high computational efficiency of the proposed STA.

#### 4. Conclusions

A new algorithm is proposed for solving the  $k - \omega$  turbulence equations embedded in the ocean general circulation model (OGCM). The algorithm is based on the multicomponent splitting method. The equations of turbulence are split into the two stages: 1) three-dimensional transport–diffusion and 2) local generation–dissipation. At the generation–dissipation stage, the equations are solved analytically, which increases computational efficiency. The method makes it possible to use the time step of the OGCM to solve the turbulence equations.

The use of an analytical solution of the  $k - \omega$  turbulence model equations opens up new possibilities for simulation of the ocean hydrophysical characteristics. The obtained results showed the ability of the new algorithm to increase the adequacy of reproducing ocean characteristics by variations in the analytical solution coefficients. These variations make it possible to study the sensitivity of the solution to the input parameters of the model more fully. Estimations are given of sensitivity to variations in the TKE inflow at the ocean surface. High sensitivity of the ocean vertical structure to variations in the coefficients in the analytical solution is revealed.

Stability of the ocean upper layer stratification in the Arctic basin is mainly related to the salinity vertical distribution. The use of stability functions on the basis of solving the Reynolds equations in the coefficients of the analytical solution (3) improves the reproduction of the upper desalination layer in comparison with using the simple form of the Prandtl number dependence on the Richardson number.

It is shown that the UQL thickness during the free convection development in the North Atlantic and the Arctic Ocean is highly sensitive to variations in the coefficients  $A$  and  $B$  of the analytical solution (3). It can vary by tens of meters in the mid-latitudes and hundreds of meters in the Nordic Seas, depending on the realistic variations of these coefficients.

### Acknowledgments

The research was carried out in the INM RAS with the support of the Russian Science Foundation (grant No. 17-77-30001) and the Russian Foundation for Basic research (grants No. 18-05-00177 and No. 16-05-00534).

### References

- [1] Volodin E, Galin V, Gritsun A, Gusev A, Diansky N, Dymnikov V, Ibrayev R, Kalmykov V, Kostykin S, Kulyamin D, Lykossov V, Mortikov E, Rybak O, Tolstykh M, Fadeev R, Chernov I, Shashkin V and Iakovlev N 2016 *Mathematical modelling of the Earth system* (MAKS Press, Moscow State University, Moscow)
- [2] Warner J, Sherwood C, Arango H and Signell R 2005 *Ocean Modelling* **8** 81–113
- [3] Noh Y, Ok H, Lee E, Toyoda T and Hirose N 2016 *J. Phys. Oceanogr.* **46** 57–78
- [4] Canuto V, Howard A, Cheng Y, Muller C, Leboissetier A and Jayne S 2010 *Ocean Modelling* **34** 70–91
- [5] Zaslavskii M, Zalesny V, Kabatchenko I and Tamsalu R 2006 *Oceanology* **46** 159–69
- [6] Mellor G and Yamada T 1974 *J. Atm. Sci.* **31** 1791–806
- [7] Burchard H, Bolding K and Villarreal M 1999 *GOTM, a General Ocean Turbulence Model: Theory, Implementation and Test Cases*. EUR/European Commission (Space Applications Institute)
- [8] Blanke B and Delecluse P 1993 *J. Phys. Oceanogr.* **23** 1363–88
- [9] Moshonkin S, Alekseev G, Bagno A, Gusev A, Diansky N and Zalesny V 2011 *Russ. J. Num. Anal. Math. Modelling* **26** 161–78
- [10] National Geophysical Data Center, NOAA 2006 *2-minute Gridded Global Relief Data (ETOPO2) v2* national Geophysical Data Center
- [11] Large W and Yeager S 2009 *Clim. Dyn.* **33** 341–64
- [12] Locarnini R, Mishonov A, Antonov J, Boyer T, Garcia H, Baranova O, Zweng M and Johnson D 2010 *NOAA Atlas NESDIS 68* World Ocean Atlas 2009 ed Levitus S (Washington, D.C.: U.S. Government Printing Office) 184 pp.
- [13] Antonov J, Seidov D, Boyer T, Locarnini R, Mishonov A, Garcia H, Baranova O, Zweng M and Johnson D 2010 *NOAA Atlas NESDIS 69* World Ocean Atlas 2009 ed Levitus S (Washington, D.C.: U.S. Government Printing Office) 184 pp.
- [14] de Boyer Montégut C, Madec G, Fischer A, Lazar A and Iudicone D 2004 *J. Geophys. Res. Oceans* **109** C12003